Chemical Grafting of Highly Dispersed VO_x/CeO_2 for Increased Catalytic Activity in Methanol Oxidative Dehydrogenation

Berlin Sudduth[1] · Junming Sun[1] · Yong Wang[1,2]

Abstract

Vanadia supported on well-defined ceria nanocubes are synthesized at various loadings using a liquid-phase chemical grafting technique and are compared to those prepared using traditional incipient wetness impregnation. Raman and IR characteriza-tion reveal that, as vanadia loading is increased to near monolayer coverage, vanadia deposited using grafting shows greatly enhanced dispersion (i.e., improved VO_x monomer/dimer distribution). Methanol is used as a probe molecule to explore the redox behavior of the catalysts. IR and temperature programmed desorption of methanol show increased CO_2 formation occurs on the bare ceria support and increasing the dispersion of vanadia promotes dehydrogenation to formaldehyde due to the inhibited oxygen vacancy formation on VO_x/CeO_2. Hydrogen temperature programmed reduction demonstrates that the catalyst reducibility and formation of surface oxygen vacancy are directly related to the degree of vanadia oligomeriza-tion. The samples prepared using grafting exhibit superior catalytic performance for methanol oxidative dehydrogenation to formaldehyde compared to the impregnated samples, due to the presence of highly dispersed VO_x species (i.e., monomers and dimers).

Graphical Abstract

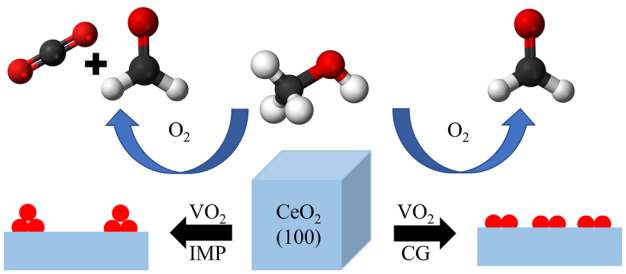

Keywords Ceria · Supported VO_x catalysts · Chemical grafting · Methanol · Oxidative dehydrogenation

1 Introduction

Metal oxide supported vanadia catalysts are among the most studied oxidation catalysts for a variety of redox reactions such as oxidative dehydrogenation (ODH) of alcohols and short-chain alkanes [1–9]. Ceria (CeO_2) supported vanadia has been of particular interest because CeO_2's reducibility, oxygen storage capacity, and oxygen mobility result in it outperforming other metal oxide supports in oxidation reactions [7, 10]. Various molecular structures of vanadia can be formed depending on the metal oxide support and loading. The structure of these vanadia species has been studied

✉ Yong Wang
yong.wang@pnnl.gov

[1] The Gene and Linda Voiland School of Chemical Engineering and Bioengineering, Washingston State University, Pullman, WA 99164, USA

[2] Institute for Integrated Catalysis, Pacific Northwest National Laboratory, Richland, WA 99354, USA

using a variety of techniques including Raman [11–16], IR [10, 17–19], UV–Vis diffuse reflectance spectroscopy (UV–Vis DRS) [19–24], ^{51}V MAS NMR [25–27], X-ray absorption fine-structure spectroscopy (XANES/EXAFS) [9, 22, 28], X-ray photo-electron spectroscopy (XPS) [18, 19, 26, 29–31], and scanning tunneling microscopy (STM) [32]. The catalytic performance of these vanadia species has been extensively studied on polycrystalline CeO_2 using methanol ODH as a simple redox probe reaction [4, 7, 33–35]. Bulk V_2O_5 nanoparticles perform much worse than dispersed vanadia due to the former's poor reducibility and decreased exposure of vanadia surface sites. The relative activities of the vanadia monomers, dimers, and trimers have shown little to no difference in certain polycrystalline studies [2, 36].

Surface science techniques and computational studies have allowed for atomic-level understanding of the metal oxide surface structure and the deposited vanadium species [37–41]. Unlike some of the previous polycrystalline studies, these studies suggest that monomeric vanadia is more active than polymeric species for low temperature methanol ODH. Temperature programmed desorption (TPD) of methanol on vanadia deposited on well-ordered CeO_2(111) thin films displayed a lower formaldehyde (CH_2O) desorption temperature from isolated vanadia than from two-dimensional oligomers [38]. A density function theory (DFT) study comparing monomeric and a trimeric vanadia species on CeO_2 showed a similar trend with CH_2O able to form at lower temperatures on vanadia monomers while the intrinsic reaction barriers on trimers was greater and actually much more similar to that of pristine CeO_2(111) [42]. This was attributed to increased mobility of surface O after structural relaxation associated with vanadia monomers. Limitations in differentiating monomeric and oligomeric vanadia species in polycrystalline studies may be caused by the heterogeneous nature of CeO_2 nanoparticles and poor control of vanadia deposition.

CeO_2 nanoshapes synthesized with well-defined morphologies have been used to develop surface–function relationships in nanoparticle catalysis and correlate these results with those found from surface science and theoretical approaches [43, 44]. Nanoshapes such as rods, octahedra, and cubes have been shown to expose specific facets of the CeO_2 crystal surface which provide different anchoring sites for deposited vanadia. Studies of VO_x/CeO_2 using these nanoshapes have shown that changing the CeO_2 morphology can impact vanadia dispersion, methoxy species formed after methanol adsorption, and methanol ODH activity [14, 15, 45, 46]. This suggests that the heterogeneity of polycrystalline VO_x/CeO_2 may not be suitable to accurately probe the catalytic properties of each dispersed vanadia species, as their individual characteristics are obscured by the presence of many different combinations of VO_x and CeO_2 structures.

Many different deposition methods are used when synthesizing supported vanadia materials with aqueous impregnation of vanadium oxalate being the most often used commercially. Other methods include dry impregnation of crystalline V_2O_5, vapor phase grafting with $VOCl_3$, and nonaqueous impregnation with vanadium alkoxides [11]. Though many different techniques have been used, the influence of the preparation method on vanadia structures is not completely clear. Earlier studies suggest that the high mobility of hydrated vanadia species results in the redispersion of surface vanadia to form a monolayer and minimize the surface free energy of the support [2]. Facile vanadia migration, observed to begin as low as 450 °C on VO_x/TiO_2, was used to explain why preparation method had no observable impact on the calcined VO_x structure though it has been suggested that the preparation method affects the rate of VO_x migration [47, 48]. Grafting processes offer the potential for atomic-level control of supported species and have been shown to double the rate of propane ODH [49]. A unique liquid phase method has been developed for grafting various metal oxides onto the surface of mesoporous silica (SiO_2) [50–52]. Due to vanadia's poor interaction with SiO_2, the method could not directly introduce vanadia onto SiO_2, but by first depositing titania onto the SiO_2 to act as anchoring points, the method was successful and proved it could be used for other metal oxide supports. Supported vanadia catalysts deposited under anhydrous conditions displayed greater dispersion than those synthesized using conventional impregnation which resulted in significantly increased rates of ethanol partial oxidation [53]. Recent work has employed similar surface organometallic chemistry for liquid [54] and gas [55] phase grafting of dispersed vanadia onto SiO_2 supports. These studies suggest that anhydrous preparation methods may significantly enhance the dispersion of supported vanadia species that remain stable after synthesis.

In the present work, a series of VO_x/CeO_2 catalysts were prepared via incipient wetness impregnation and liquid phase chemical grafting over a range of vanadia loadings: below, near, and above monolayer coverage. CeO_2 nanocubes were chosen as the support because these nanoshapes have demonstrated greater VO_x dispersion on their (100) facets than nanorods or octahedra [45]. The nanocubes were synthesized for maximum particle size to provide large, uniform terraces as anchoring sites for vanadia while minimizing the density of defect sites on the surface [56]. In addition to contributing to heterogeneity in anchoring sites, CeO_2 surface defects are shown to react more readily with supported vanadia to form cerium(Ill) orthovanadate ($CeVO_4$) [14]. Through a variety of spectroscopic techniques, it is demonstrated that grafting increases vanadia dispersion and, using methanol ODH as a probe reaction, these dispersed vanadia species are more active for catalytic oxidation.

2 Experimental

2.1 Catalyst Preparation

The CeO_2 nanocube supports were synthesized via a hydrothermal method using 36 g $Ce(NO_3)_3$•$6H_2O$ (Sigma-Aldrich, 99.99%) and 2.17 g NaOH (Sigma-Aldrich, ≥ 97%) [57]. The $Ce(NO_3)_3$•$6H_2O$ was dissolved in a 350 mL aqueous solution and the NaOH was dissolved in a 50 mL aqueous solution. The NaOH solution was added dropwise to the cerium solution and mixed at room temperature for 30 min. The mixture was then poured into four separate 125 mL Teflon liners and placed in autoclaves (Parr Instrument Company, large capacity acid digestion vessel) to be heated to 180 °C (10 °C/min) for 24 h. The CeO_2 precipitate was separated via centrifuge before being washed three times with deionized water and ethanol in an ultrasonic bath. The rinsed precipitate was treated to additional washes to remove any remaining Na impurities [58]: a solution of 0.1 M NH_4OH, three additional water rinses, followed by washing with a 0.1 M HNO_3 solution and three final water rinses. The treated precipitate was dried for 12 h at 50 °C before calcination at 450 °C for 4 h in air.

VO_x was deposited on the CeO_2 supports using either impregnation (IMP) or chemical grafting (CG). Before impregnation, the CeO_2 support was pretreated at 450 °C for 30 min and then cooled to room temperature. A solution of ammonium metavanadate (NH_4VO_3, Sigma-Aldrich, ≥ 99%) was prepared by dissolving the vanadium precursor in an aqueous solution of oxalic acid ($C_2H_2O_4$, Sigma-Aldrich, ≥ 99%) at a NH_4VO_3:$C_2H_2O_4$ molar ratio of 1:2. The vanadium solution was deposited on the CeO_2 support using incipient wetness impregnation, dried for 12 h at 50 °C, and calcined at 450 °C in air for 4 h [45]. A liquid phase chemical grafting method was used to deposit vanadium onto the CeO_2 supports [53]. Approximately 0.3 g CeO_2 is pretreated at 450 °C for 30 min in air before being transferred to a flask containing 100 mL anhydrous toluene (Sigma-Aldrich, 99.8%). The mixture was refluxed under N_2 (20 mL/min) and continuous stirring for 3 h for further dehydration. The temperature of the mixture was decreased to 60 °C before adding vanadium oxytriisopropoxide (VOTP, Sigma-Aldrich) corresponding to the desired vanadium loading. The solution continues to mix at 60 °C for 15 h under N_2 before being cooled to room temperature. The VO_x/CeO_2 was separated from the remaining liquid via centrifuge and washed with anhydrous toluene three times to remove any unreacted vanadium precursor. Finally, the sample was dried for 12 h at 50 °C before calcination at 450 °C for 4 h in air. The prepared VO_x/CeO_2 catalysts are denoted as V-IMP and V-CG for samples prepared via impregnation and chemical grafting, respectively. The various vanadium loadings for each sample are denoted as xV with x being the vanadium atom density (i.e., 5 V represents a sample with 5 V atoms/nm^2 ceria support). Monolayer surface coverage of vanadia on CeO_2 is reported to be between 5 and 7 V/nm^2 [2, 15]. The vanadia loadings chosen for this study were 1, 5, and 8 V/nm^2 to represent low, near monolayer, and above monolayer coverages. Three separate batches of the 1 and 5 V/nm^2 impregnated and grafted samples were synthesized using the same CeO_2 support to test the reproducibility of the deposition methods.

2.2 Material Characterization

Transmission electron microscopy (TEM) analysis of the calcined CeO_2 supports was performed to confirm their morphology and particle size using an FEI Technai G2 20 Twin operated at 200 kV equipped with a 4 k Eagle CCD camera. The specific surface areas (SSA) of the CeO_2 supports and VO_x/CeO_2 catalysts were determined using Brunauer–Emmett–Teller (BET) analysis of N_2 adsorption–desorption isotherms. Approximately 0.5 g of each sample was placed in quartz tubes and degassed under vacuum at 300 °C for 3 h before BET analysis at 77 K using a Micromeritics TriStar II 3020 Physisorption Analyzer. XRD patterns are obtained using a Rigaku MiniFlex X-ray diffractometer using Cu-Kα (λ = 1.54178 Å). Normal operating power are 40 kV, 30 mA and measurements were obtained from 3° to 90° at scanning speeds of 0.5°/min. In situ Raman spectroscopy was conducted by loading approximately 50 mg of sample into an in situ reactor cell (Linkam CCR1000) and heating to 400 °C for 1 h under 10% O_2/He (20 mL/min). The dehydrated samples were cooled to 100 °C before measuring from 0 – 1600 cm^{-1} using a Raman spectroscope (Horiba LabRAM HR 800) equipped with a 532 nm (Ventus LP 532) laser source and Synapse CCD (charge-coupled device) detector.

IR spectra were collected using diffuse reflectance infrared Fourier transform spectroscopy (DRIFTS) with a Bruker Tensor 27 FTIR spectrometer equipped with a Harrick Praying Mantis attachment, averaging 256 scans with a spectral resolution of 4 cm^{-1}. Analyses of the bare catalysts were done by first pretreating the samples at 400 °C for 1 h under 10% O_2/He flow (20 mL/min) and cooling to 150 °C before spectral acquisition under 5% Ar/He flow (20 mL/min). The bare catalyst vibrations are difference spectra using potassium bromide (KBr) at 150 °C as the reference background. Methanol adsorption was conducted after acquisition of the bare sample spectra by lowering the temperature to 50 °C and flowing 5% Ar/He (10 mL/min) through a bubbler containing methanol (Sigma-Aldrich, > 99.9%) at room temperature. Methanol was continually introduced until saturation,

as monitored by changes in the IR spectra. Samples were purged under 5% Ar/He flow (30 mL/min) for 30 min or until the methanol QMS signal stabilized and there were no further changes in the IR spectra. Samples were then heated to 450 °C (10 °C/min) under 5% Ar/He flow (30 mL/min) while taking spectra at various temperatures. Spectra collected during desorption are difference spectra referenced to the pretreated catalyst at the same temperature, before methanol adsorption, as the background.

H_2 temperature-programed reduction (H_2-TPR) was performed using an AutoChem II 2920 Chemisorption Analyzer (Micromeritics) equipped with a thermal conductivity detector (TCD). Approximately 50 mg of catalyst was loaded into a quartz fixed bed reactor for analysis. Samples were pretreated by heating to 400 °C (10 °C/min) under 10% O_2/He flow (50 mL/min) for 30 min before cooling to ambient temperature and purging with 5% Ar/He flow (50 mL/min) for 30 min. The gas flow was then switched to 10% H_2/Ar (50 mL/min) and kept at ambient temperature until the TCD baseline stabilized at which point the temperature was raised to 900 °C (10 °C/min). Methanol temperature-programmed desorption (CH_3OH-TPD) was conducted on the same chemisorption equipment utilizing the online QMS (Quadra 220, Pfeiffer). Samples were loaded and pretreated using the same procedure described for H_2-TPR and cooled to 100 °C for methanol adsorption. Methanol was introduced via 0.5 mL pulses of roughly 5% CH_3OH/He generated in a flask of methanol held at room temperature with He (10 mL/min) bubbled through until saturation. Samples were then purged under 5% Ar/He flow (50 mL/min) for 2 h or until the TCD baseline stabilized before increasing the temperature to 600 °C. The various desorption products were monitored using QMS with the following m/z values: methanol (31), formaldehyde (30), dimethyl ether (45), carbon dioxide (44), carbon monoxide (28), water (18), and hydrogen gas (2). Each desorbed QMS signal was normalized by the argon (m/z = 40) signal from the 5% Ar tracer in the carrier gas.

2.3 Methanol Oxidative Dehydrogenation

Steady-state methanol ODH reactions were carried out in a fixed-bed flow reactor to evaluate catalytic performance. Approximately 25 mg of catalyst sieved between 0.250 and 0.149 mm were diluted with inert silicon carbide (SiC) at a 1:20 catalyst:SiC mass ratio to prevent mass transfer limitations and temperature gradients. A K-type thermocouple with quartz lining was inserted into the catalyst bed for accurate sample temperature control. Samples were pretreated after being loaded into the reactor by increasing the temperature to 400 °C (10 °C/min) for 30 min under 10% O_2/He (100 mL/min) before lowering the furnace to the desired temperature. Methanol was introduced using a syringe pump which injected the liquid methanol upstream of the catalyst into piping heated to 60 °C to ensure complete evaporation before reaching the reactor. The feed gas during reaction consisted of 3% methanol, 10% O_2, and 87% He with a total gas flow rate of 100 mL/min. Reactor products were heated to 70 °C to prevent condensation and analyzed using an online Micro-GC (Agilent 490) equipped with four columns (Molsieve, CP-PoraPLOT U, aluminum oxide column and CP-Sil 5 CB) using TCD. Reaction rates were analyzed under differential kinetic conditions (conversions below 10%) and normalized to turnover frequencies (TOF) based on the vanadium atom loaded as determined by ICP-MS. Separate steady state experiments were conducted at 240 °C to measure selectivity at higher conversions. A target conversion of 50% was obtained by controlling the gas hour space velocity (GHSV) between 80,000 and 240,000 h^{-1}. Samples were again diluted with the 1:20 catalyst:SiC mass ratio and the reactant gas maintained the same MeOH:O_2:He mole ratio as the previous conditions. Reactivities were measured on the three separate batches of impregnated and grafted samples to determine the variance in their performance.

3 Results and Discussion

3.1 Physical and Structural Properties

XRD of the calcined CeO_2 support (Fig. 1a) Show that the CeO_2 nanocubes exhibit a pure cubic fluorite structure with no detectable peaks from $Ce(OH)_3$ or $Ce(OH)CO_3$ impurities indicative of sufficient calcination of the cerium precursor [57]. Using the Scherrer equation based on the XRD patterns, the average crystallite size is 37 nm. TEM imaging, as seen in Fig. 1b, shows the cubic morphology of the calcined CeO_2 support. Based on the TEM images, there are a distribution of particle sizes with an average particle size of 44 nm, which is in relative agreement with the particle size determined using XRD. High-resolution images of cubes synthesized using the same procedure can be found in a previous paper where the surfaces were determined to expose the (100) facet by measuring the interplanar distance of the lattice fringes [56]. The specific surface areas and vanadia loadings for the CeO_2 and VO_x/CeO_2 are summarized in Table 1. The CeO_2 nanocubes have a specific surface area of 10.3 m^2/g which is in agreement with previous materials synthesized using the same procedure [56]. There is only a minor decrease in surface area with increased vanadia loading. Inductively coupled plasma mass spectrometry (ICP-MS) measurements of the vanadia loadings were made for the catalysts whose vanadia remained as VO_x surface species (1 and 5 V/nm^2) and, as shown in Table 1, demonstrate that the actual vanadia loadings agreed with the expected loading during synthesis.

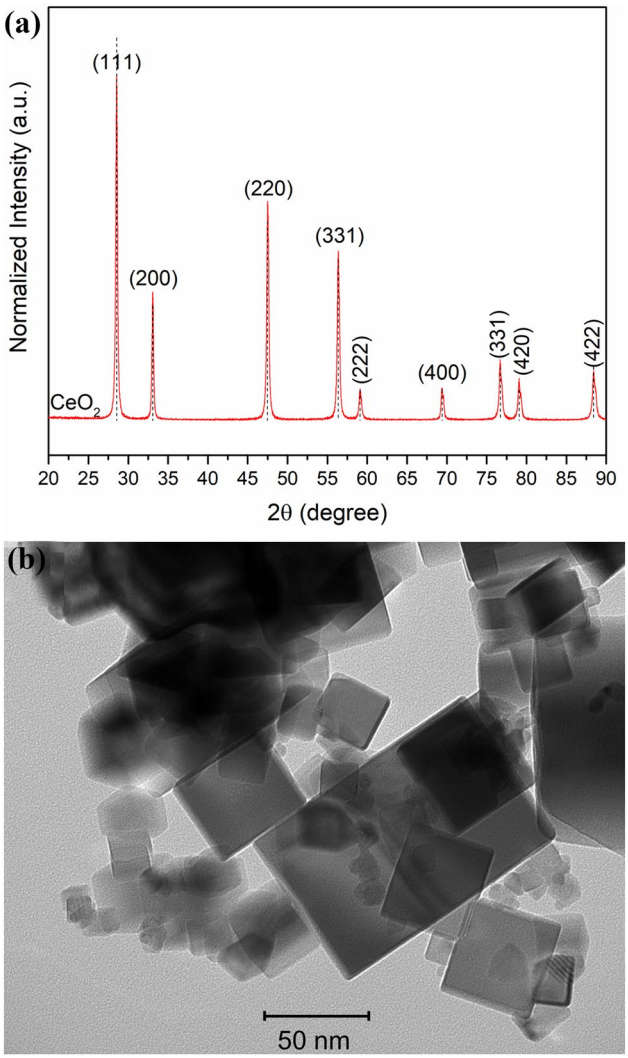

Fig. 1 **a** XRD pattern and **b** TEM image of CeO_2 nanocubes after calcination at 450 °C used as the vanadia support

The Raman spectra for the dehydrated catalysts with various vanadia loadings are presented in Fig. 2. Spectra were normalized by the intensity of the F_{2g} mode of CeO_2's fluorite phase at 460 cm^{-1}, which can be seen in the full spectra (Fig. S1) [59]. At the lowest vanadia loadings for both the grafting and impregnated samples a single feature at 1005 cm^{-1} is observed. With an increase in vanadia loading to near monolayer (5 V/nm^2) there is a decrease in the intensity of the 1005 cm^{-1} band along with the observation of two new bands at 1019 and 1036 cm^{-1}. A direct structure-spectroscopy relationship was established in a model $VO_x/CeO_2(111)$ system combining infrared reflection absorption spectroscopy (IRAS), STM, and DFT [32], assigning the V=O stretches for monomers and trimers at 1006 and 1033 cm^{-1}, respectively. Raman analysis of CeO_2 nanoparticle supported VO_x has shown similar V=O bands in the region between 1000 and 1050 cm^{-1} with features

Table 1 Summary of physical properties of CeO_2 and VO_x/CeO_2 catalysts

Sample	Particle size(nm)[a]	SSA (m^2/g)	V density (V/nm^2)	V loading (wt%)[b]	V loading (wt%)[c]
CeO_2	44	10.3	–	–	–
1V-CG-CeO_2	–	10.0	1	0.09	0.16
5V-CG-CeO_2	–	9.8	5	0.44	0.41
8V-CG-CeO_2	–	9.5	8	0.70	–
1V-IMP-CeO_2	–	10.1	1	0.09	0.15
5V-IMP-CeO_2	–	10.0	5	0.44	0.40
8V-IMP-CeO_2	–	9.4	8	0.70	–

[a]Estimated average from TEM images

[b]Estimated from synthesis conditions

[c]Measured using ICP-MS

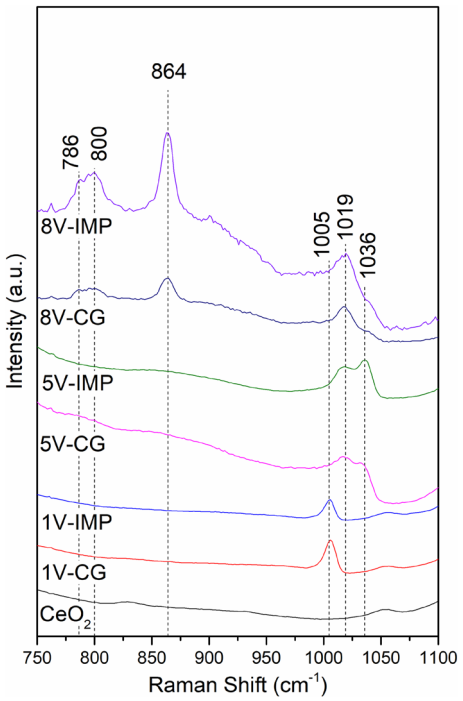

Fig. 2 Vanadium region of the Raman spectra for CeO_2 nanocube supports and VO_x/CeO_2 catalysts at various loadings deposited via chemical grafting and impregnation

at ~ 1015 cm^{-1} tentatively assigned to VO_x dimers [14, 16, 60]. Based on these studies the bands observed at 1005, 1019, and 1036 cm^{-1} are assigned to monomers, dimers, and trimers or larger 2-D VO_x species, respectively. Weak and broad features centered approximately at 710 and 850 cm^{-1}

appear on the samples with vanadia loadings of 5 V/nm^2 and greater and can be attributed to Ce–O–V bridging modes of isolated vanadia species [15, 40]. A comparison of the two 5 V/nm^2 samples prepared with grafting and impregnation shows that the trimeric V=O band is dominant on the impregnated catalysts while the dimeric V=O band dominates the grafting-prepared catalysts. This observation suggests that chemical grafting is beneficial to the improved dispersion of vanadium at higher V loadings. A semi-quantitative analysis of the VO_x species over the impregnated catalyst, using the intensities of the three V=O Raman bands (deconvolution of the spectra shown in Fig. S2), suggests that only 5% of the vanadium is monomeric with 55% and 40% being dimeric and trimeric VO_x species, respectively. In contrast, the grafted vanadia is significantly more disperse with monomeric VO_x representing 25%, 55% comprised of dimeric species, and only 20% remaining as trimeric species.

Previous studies have suggested that the method of preparation does not have a significant impact on the final structure of supported VO_x due to low temperature redispersion of bulk V_2O_5 on metal oxide supports below monolayer coverage [2]. Redispersion of any possible bulk V_2O_5 is consistent with the Raman observations showing no bulk V_2O_5 formation but only monomers and two-dimensional oligomers, up to near monolayer coverage, regardless of the preparation method. The mechanism of vanadia redispersion is believed to occur via crystalline V_2O_5 forming a mobile amorphous V_2O_5 phase at low temperatures which easily diffuses across the support, approaching a monolayer structure of highly oligomerized 2-D species across the support to minimize surface energy [48]. Compared to amorphous V_2O_5, isolated VO_x species such as monomers and dimers are more stable, resisting oligomerization under higher calcination temperatures [14]. Even then, study of the hydrated VO_x species formed upon exposure to ambient moisture suggested that these species are highly mobile and the resulting VO_x structures are thermodynamically controlled and may not be influenced by preparation method [47, 61]. Herein, the improved dispersion observed for the near monolayer grafted catalysts is consistent with the results of grafting vanadia on SiO_2 under anhydrous conditions [53–55]. The persistent, increased dispersion may be a result of the chemical grafting reaction between the vanadium precursor and CeO_2 support, which may form more stable vanadia complexes, so the improved dispersion is maintained after calcination. While exposure to ambient moisture after the initial anhydrous grafting deposition may have resulted in some redistribution of the surface vanadia, the method of preparation clearly influences the structure of the resulting VO_x species.

Increasing the vanadia loading above monolayer coverage introduces a distinct band at 864 cm^{-1} which sits above the broad Ce–O–V background of the 8 V/nm^2 catalysts and is attributed to the symmetric stretching mode $\nu_1(A_{1g})$ of VO_4 in $CeVO_4$. A weaker feature centered around 790 cm^{-1} can be assigned to the overlap of $CeVO_4$'s two asymmetric stretching modes $\nu_3(B_{1g})$ and $\nu_3(E_g)$ observed at 786 and 800 cm^{-1}, respectively [62]. With the formation of the $CeVO_4$ phase, a significant decrease of trimeric VO_x at 1036 cm^{-1} is observed. $CeVO_4$ has been shown to form from the reaction of surface vanadia with CeO_2 supports [14, 15]. The formation of $CeVO_4$ depends on the loading of vanadia and calcination temperature. At lower vanadia loading, highly dispersed VO_x species tend to form, which have been shown to be stable up to 800 °C on cubes at 2 V/nm^2 [14]. With higher vanadia loading, however, oligomerized VO_x species form, which react with CeO_2 at lower temperatures [63]. When the vanadia loading is increased from 5 to 8 V/nm^2, the increased oligomerization of vanadia may lead to the enhanced formation of $CeVO_4$ at the expense of the larger 2-D VO_x species (1036 cm^{-1}). In comparison, the V = O features associated with monomeric and dimeric VO_x are largely unchanged, suggesting that they are stable at 8 V/nm^2 after calcination at 450 °C. A comparison of the impregnated and grafted samples shows considerably greater intensities of the bands associated with $CeVO_4$ for the impregnated catalyst, due to the expected higher fraction of oligomerized VO_x species.

CeO_2 defect density has been shown to be a strong indicator of MeOH ODH activity with more defective nanoshapes displaying increased TOFs and decreased activation energies [45, 56].The interaction between CeO_2 defect sites and deposited vanadia can been investigated by the changes in defect density which is determined using the ratio of the intensity of the f_{2g} peak (460 cm^{-1}) and the peak associated with defects (592 cm^{-1}) (I_D/I_{F2g}) [14, 15]. The defect densities using impregnation and grafting are shown in Fig. 3. Both deposition methods result in decreased (I_D/

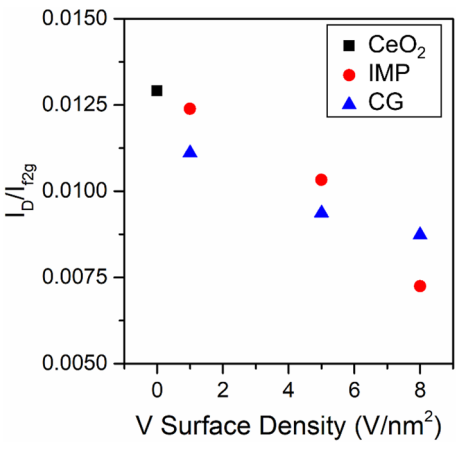

Fig. 3 Plot of the band intensity ratios between the defect and f_{2g} Raman modes with respect to vanadia surface density

I_{F2g}) ratios with VO_x loading. This suggests that vanadia addition interacts with surface defects by either eliminating them or inhibiting their formation. The strong interaction between CeO_2 defects and VO_x has been demonstrated in extensive multiwavelength Raman studies of CeO_2 supports which have varying defect densities over a range of VO_x loadings [15, 60]. This inhibition will be further confirmed in the following studies of redox properties of the samples (i.e., H_2-TPR). The role of defects during the chemical grafting reaction and the strong metal-support interaction that leads to $CeVO_4$ formation may also impact the stability of dispersed VO_x on CeO_2.

The impact of the synthesis method was further explored by IR analysis of surface hydroxyl groups before and after VO_x deposition. Figure 4 displays DRIFTS spectra in the OH stretching region (ν_{OH} = 4000–3200 cm^{-1}) for the CeO_2 support and VO_x/CeO_2 catalysts. Three bands are observed on bare CeO_2 nanocubes: the highest frequency band at 3711 cm^{-1} corresponds to terminal OH while two overlapping bands at 3638 and 3621 cm^{-1} represent bridged hydroxyl groups [64, 65]. The broad band centered around 3506 cm^{-1} is attributed to residual cerium oxyhydroxide trapped in the support's pores which do not interact with the deposited VO_x [64]. As VO_x is deposited and its loading increased, there is a general decrease in the intensity of the bands associated with surface OH on bare CeO_2 until they completely disappear at above monolayer coverage (8 V/nm^2). An additional peak around 3739 cm^{-1} appears upon VO_x deposition and becomes more prominent at near monolayer coverage (5 V/nm^2). As this high frequency band

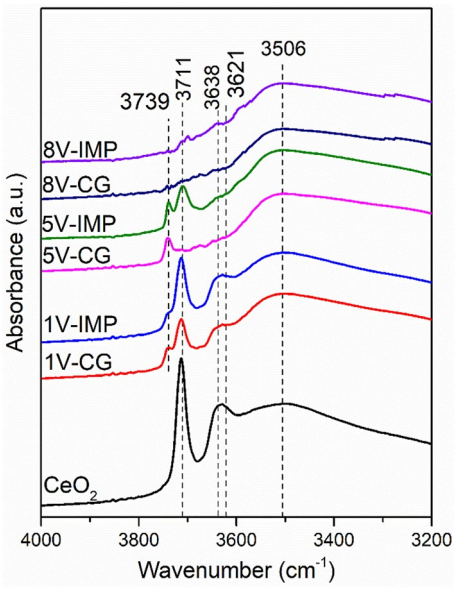

Fig. 4 DRIFTS spectra in the hydroxyl group region of dehydrated CeO_2 support and VO_x/CeO_2 catalysts with varying VO_x surface densities

increases up until moderate coverage but disappears as the CeO_2 support is completely covered, it may be attributed to surface hydroxyl groups associated with nearby VO_x. A comparison of the surface hydroxyls groups remaining after grafting and impregnation at equal VO_x loadings shows that the chemically grafted VO_x titrates the surface hydroxyl groups to a greater extent. At 5 V/nm^2 the surface hydroxyl groups associated with bare CeO_2 completely disappear whereas the impregnated sample at the same VO_x loading maintains a significant band for terminal hydroxyl groups. The better titration of hydroxyl groups using grafting can be attributed to the more efficient condensation reaction between the CeO_2 support's surface hydroxyls and VOTP during the liquid phase chemical grafting process. The greater decrease in remaining CeO_2 hydroxyl in comparison to impregnation is consistent with the Raman analysis showing that vanadia on the grafted catalysts are highly dispersed whereas those on the impregnated samples are more oligomerized leaving additional un-titrated hydroxyl groups on the surface.

3.2 DRIFTS of MeOH

DRIFTS analysis was conducted to study the methanol adsorption, reaction, and desorption as a function of temperature. Figure 5 contains the DRIFTS spectra obtained during methanol TPD from the bare CeO_2 support and the near monolayer VO_x/CeO_2 catalysts. The 5 V/nm^2 catalysts deposited using grafting and impregnation were chosen because, as shown in the previous section, they demonstrated the greatest differences in structural properties between the two synthesis methods. Methanol dissociatively adsorbs on the bare CeO_2 at 50 °C to form methoxy on the surface. As seen in Fig. 5a, two peaks at 1102 and 1041 cm^{-1} dominate the ν(CO) region that are attributed to terminal and bridged methoxy on CeO_2, respectively [46], while the hydroxyl bending mode of adsorbed methanol (δ(OH)) may contribute to the band at 1357 cm^{-1} [10]. In the ν(CH) region, the two most intense peaks at 2917 and 2815 cm^{-1} are assignable to the asymmetric and symmetric CH_3 stretching modes of methoxy, respectively. The two shoulders at 2954 cm^{-1} and 2841 cm^{-1} are characteristic of physisorbed methanol. The formation of formate species is also detected, as evidenced by the ν_{as}(OCO) vibration at 1571 cm^{-1} and the ν_s(OCO) band at 1357 cm^{-1}. As the desorption temperature increases the peaks associated with physisorbed methanol should disappear but features remain in these regions at high temperatures because they overlap with formate C–H stretching at 2934 cm^{-1} and 2841 cm^{-1} and are not removed until formate completely decomposes between 400 and 450 °C. Methoxy desorbs from the CeO_2 surface between 350 and 400 °C as indicated by the removal of its associated $\nu(CH_3)$ and ν(CO) modes.

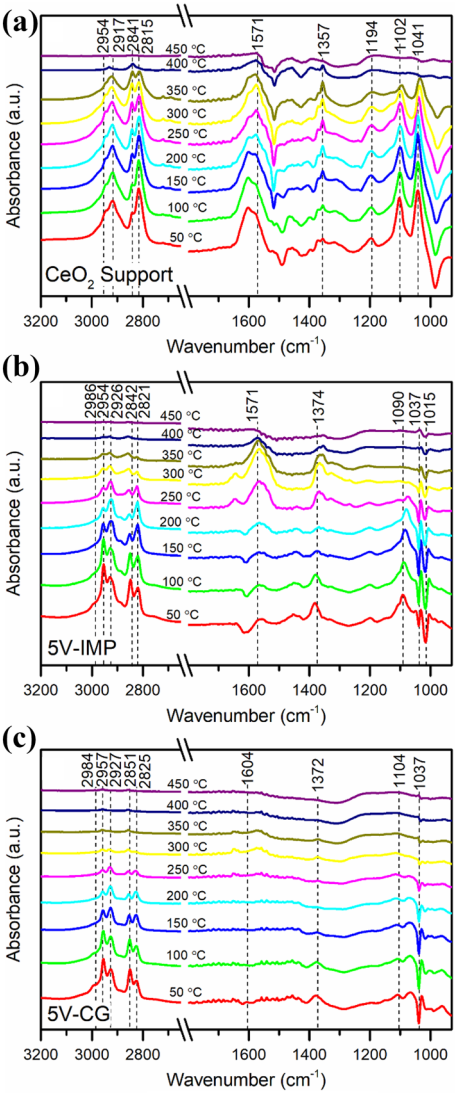

Fig. 5 DRIFTS spectra following adsorption of MeOH and purging at 50 °C on **a** CeO_2 nanocubes and VO_x/CeO_2 catalysts deposited using **b** impregnation and **c** chemical grafting, and then heating to higher temperatures under He

The DRIFTS spectra of the 5 V/nm^2 impregnated sample (Fig. 5b) share many of the same features as the bare CeO_2 support. After purging at 50 °C a single feature attributable to the ν(CO) mode of terminal methoxy is apparent at 1090 cm^{-1}. The ν(CO) mode of bridged methoxy, seen at 1037 cm^{-1} is no longer detectable after VO_x impregnation. In its place is one of the two new negative peaks at 1037 and 1015 cm^{-1} which are assigned to V=O of the deposited VO_x dimers and trimers, consistent with their position in the Raman spectra (Fig. 2). These peaks are negative due to interactions between VO_x and the adsorbed methanol or the evolved methoxy species [38]. Unlike the bare CeO_2, formate's characteristic vibration at 1571 cm^{-1} is barely detectable at 50 °C. Instead, additional peaks appear at 2954 and 2842 cm^{-1} after VO_x deposition in the ν(CH) region, which are attributable to the $\nu_{as}(CH_3)$ and $\nu_s(CH_3)$ modes of methoxy interacting with VO_x [10]. The presence of weaker peaks at 2954 and 2821 cm^{-1}, consistent with the modes of methoxy on the bare CeO_2, suggests that a portion of the methoxy is not associated with the deposited VO_x. As the temperature is increased, the intensity of the ν(CO) mode of formate increases up to 300 °C before decreasing until it has been completely decomposed by 450 °C. The desorption temperature of the methoxy and its reaction products appears to be lower for methoxy associated with VO_x as these modes largely disappear by 350 °C while the modes associated with bare CeO_2's persist until 400 °C.

The differences between the 5 V/nm^2 impregnated catalyst's spectra and those of the bare support seem to be exaggerated for the grafted catalyst. As shown in Fig. 5c, there are no apparent features in the ν(CO) region of the 5 V/nm^2 grafted sample after adsorption nor during the temperature increase. Methanol and methoxy clearly interact with the deposited VO_x as can be seen in the negative peak at 1037 cm^{-1} but the ν(CO) associated with neither the terminal nor bridged methoxy on CeO_2 can be detected. The characteristic ν_{as}(CO) mode of formate at 1372 cm^{-1} does not appear at 50 °C, as with the bare CeO_2, nor does it form as the temperature increases, as seen on the impregnated sample. There is a clear trend that the introduction of VO_x and an increase in its dispersion on CeO_2 suppresses the decomposition of methoxy to formate. A surface science study detected no formate on pristine, fully oxidized CeO_2(111) [66] while another study using more defective CeO_2 thin films with demonstrated methoxy species adsorbed at more coordinatively unsaturated cerium ions readily oxidized to formate species [67]. The decrease in formate species observed agrees with the decrease in defect density with increased VO_x loading, as seen in Raman (Fig. 3), and enhanced surface coverage of VO_x using chemical grafting, as seen in the nearly complete titration of CeO_2 hydroxyls (Fig. 4). In the ν(CH) region, the intensities of the asymmetrical (2957 cm^{-1}) and symmetrical (2851 cm^{-1}) modes of methoxy associated with VO_x are even stronger relative to the peaks associated to bare CeO_2. This is further evidence that depositing VO_x via grafting results in increased dispersion on the CeO_2 support. With the majority of the methoxy associated with VO_x on the grafted catalyst, the methoxy is almost completely desorbed by 300 °C.

3.3 Methanol TPD and H_2-TPR

Complementary to the DRIFTS-methanol experiments, MeOH TPD was performed in a fixed bed reactor to analyze the evolution of desorbed species with increasing temperature. Figure 6 displays the desorption profiles of every major species during MeOH TPD on the CeO_2 support and

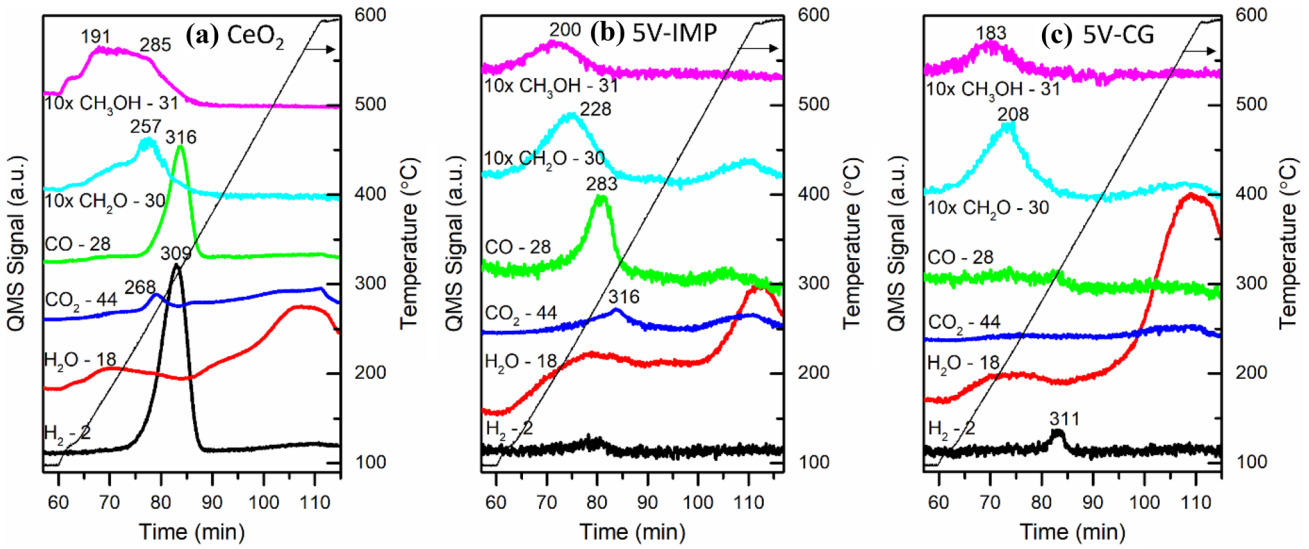

Fig. 6 TPD profiles of all major desorption products during MeOH TPD on **a** CeO_2 nanocubes and 5 V/nm$_2$ VO_x/CeO_2 catalysts deposited using **b** impregnation and **c** chemical grafting. Each species was measured using the indicated m/z signal normalized by the Ar tracer signal. QMS intensity is scaled as indicated for clarity

5 V/nm^2 catalysts, each normalized by surface area. CH_2O is the predominant product during MeOH ODH over CeO_2 and VO_x/CeO_2 at the low temperatures and conversions, so its desorption temperature is of particular interest. The CH_2O peak desorption temperature is highest for bare CeO_2 at 257 °C while the impregnated and grafted samples display peak desorption temperatures of 225 and 208 °C, respectively. This trend is consistent with DRIFTS observations of methoxy species persisting at the highest temperatures on bare CeO_2 followed by the impregnated sample and disappearing at the lowest temperatures for the grafted sample. On the grafted sample, the lower CH_2O desorption temperature may be a result of the highly dispersed VO_x species. This result is consistent with the surface science studies, which demonstrated a lower desorption-temperature of CH_2O over the VO_x of low nuclearity on CeO_2 thin films during MeOH TPD [38]. It is worth mentioning that, comparing the other desorption species, desorption from the bare CeO_2 is dominated by the complete dehydrogenation of methoxy to produce CO and H_2 at around 310 °C. While the impregnated sample produces less CO and more CH_2O at low temperature (283 °C) than bare CeO_2 does, CH_2O is the only product which desorbs from the grafting-prepared catalyst. The complete dehydrogenation of methoxy to CO can be correlated to the IR spectra which showed a significant amount of formate on bare CeO_2 that persists until high desorption temperatures, the impregnated sample displayed decreased formate on the surface which decomposed at lower temperature, and no formate was detected on the grafted surface. Increasing VO_x loading has been demonstrated to reduce the complete dehydrogenation of adsorbed methoxy [34] during methanol TPD and while the VO_x loadings of the impregnated and grafted sample are the same, the enhanced dispersion of the VO_x on the latter shows much more efficiency in modifying the sites of side reactions on the CeO_2.

H_2-TPR was used to investigate effects of deposition method on the redox properties of the VO_x/CeO_2 catalysts as shown in Fig. 7. Two broad peaks of hydrogen consumption are observed in the TPR profile of the CeO_2 support. The first begins around 322 °C with the temperature peak centered at approximately 451 °C while the second is a larger,

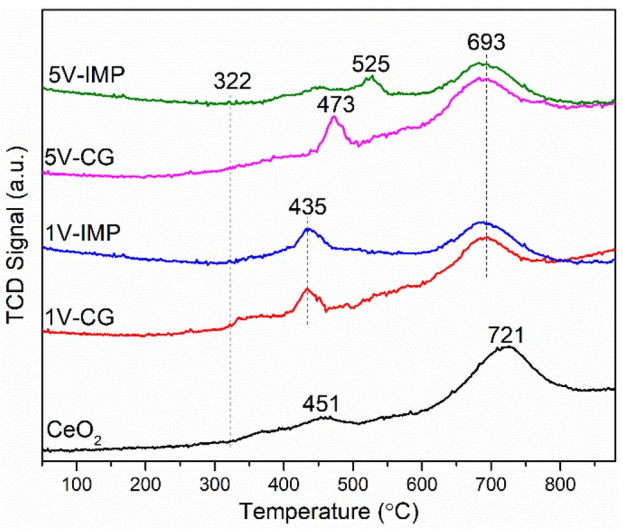

Fig. 7 H_2-TPR profiles of CeO_2 nanocube support and VO_x/CeO_2 catalysts synthesized using impregnation and chemical grafting

high temperature peak at approximately 721 °C. Reduction in the low-temperature regime (< 600 °C) is a result of removal of surface oxygen while reduction in the high-temperature one is due to removal of bulk oxygen [6, 15]. With the addition of 1 V/nm^2 using either impregnation or grafting a sharper peak at 435 °C is introduced which obscures the low-temperature reduction features (onset tail at the low temperature side) associated with bare CeO_2's surface oxygen. Studies have shown that deposited VO_x suppress the reducibility of the surface due to the stabilization of Ce^{3+} sites at the interface between VO_x and CeO_2 [63], which is consistent with the decreased oxygen vacancy observed in the Raman spectra of the samples (Fig. 3). Further increasing the VO_x loading to 5 V/nm^2 elevates the temperature of surface reduction to 473 and 525 °C for the grafted and impregnated samples, respectively, as VO_x continues to passivate the reactivity of CeO_2's surface oxygen by forming bridged bonds between them [15]. The higher reduction temperature for the impregnated sample is due to the formation highly oligomerized VO_x species (Fig. 2) which are more difficult to reduce than CeO_2's oxygen neighboring isolated VO_x [6] as shown in previous VO_x/CeO_2 studies [18, 45, 68].

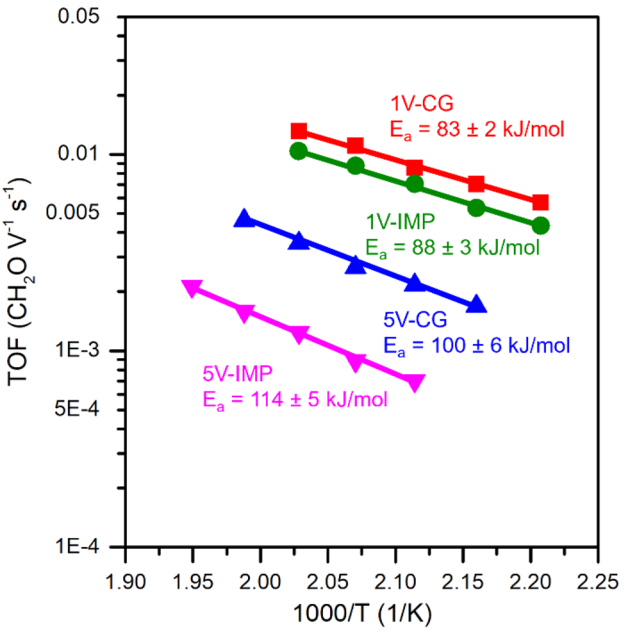

Fig. 8 Arrhenius plot of formaldehyde TOF during MeOH ODH for 1 and 5 V/nm^2 catalysts normalized by VO_x loading

3.4 Methanol ODH

Methanol ODH was chosen as the model reaction to evaluate the redox activity of the VO_x/CeO_2 catalysts. Reaction kinetics were performed under differential conditions and had a high selectivity to formaldehyde. The deep oxidation product, CO_2, was the only measurable side product and most prominent on the bare CeO_2 support (21% selectivity) with no dimethoxymethane (DMM), methyl formate (MF), nor dimethyl ether (DME) detected. The CO_2 selectivities of the VO_x/CeO_2 catalysts varied from ~ 1 to 2% for the 1 V/nm^2 samples and was undetected for the 5 V/nm^2 samples. To account for the reactivity of the CeO_2 support contributing to the overall formaldehyde production rates, the activity of bare the CeO_2 was measured under identical conditions. The rate of formaldehyde production from CeO_2 were subtracted from those measured in VO_x/CeO_2 tests according to the theoretical fraction of CeO_2 remaining exposed on the surface based on 5.5 V/nm^2 as 100% coverage [38] which is in relative agreement with the 5 V/nm^2 grafted sample nearly titrating all the surface hydroxyl groups. Turnover frequencies were measured between 180 and 240 °C with the results arranged as Arrhenius plots in Fig. 8. The MeOH ODH activity of the catalysts with low VO_x loadings (1 V/nm^2) is similar after either grafting or impregnation with apparent activation energies of 83 ± 2 and 88 ± 3 kJ/mol, respectively. Their comparable reactivity is consistent with their similarities in only displaying VO_x monomers, as evidenced in Raman, and although chemical grafting seems to titrate the surface hydroxyls to a greater extent, there were no discernable differences in redox properties investigated with H_2-TPR.

There is a significant reduction in activity when the VO_x loading is increased to 5 V/nm^2 with the grafted and impregnated catalysts displaying a three-fold and six-fold decrease in CH_2O TOFs, respectively. The apparent activation energy for the grafted sample is 100 ± 6 kJ/mol while the impregnated sample is slightly higher at 114 ± 5 kJ/mol. There is clear link between VO_x dispersion and MeOH ODH activity with the catalysts containing a higher fraction of larger oligomers displaying lower TOFs and higher activation energies. These observations are consistent with thin film studies of model CeO_2 surfaces and computational investigations which suggest VO_x monomers are most active in low temperature MeOH ODH [38, 42]. DFT calculations of MeOH ODH over a VO_x/TiO_2 system suggested that the presence of an oxygen vacancy defect site neighboring VO_x lowers the rate determining C–H breaking step [69]. The combination of decreased oxygen vacancy formation energy and fewer defects likely explains the 1 V/nm^2 catalysts displaying decreased apparent activation energies compared to the 5 V/nm^2.

Due to the overwhelming selectivity to formaldehyde at low MeOH conversions on each VO_x/CeO_2 catalyst, no clear distinctions could be made regarding the effect VO_x loading and preparation method have on selectivity. To investigate this further, separate experiments were conducted at 240 °C while varying the GHSV to maintain ~ 50% conversions. The selectivities of the CeO_2 support and VO_x/CeO_2 catalysts

are shown in Fig. 9. CH_2O continues to be the main product for each sample with CO_2 being the most prominent side product. The bare CeO_2 support has the poorest selectivity to formaldehyde (52%) which increased to ~ 74% for both 1 V/nm^2 samples. The 5 V/nm^2 impregnated sample has a CH_2O selectivity of 82% while the 5 V/nm^2 grafting-prepared sample displays the greatest selectivity of 93%. The selectivity to formaldehyde follows the same trend observed in MeOH DRIFTS and TPD analysis in which vanadia deposition and increased dispersion mitigates the complete oxidation to CO_2. A trace amount (~ 1–2%) of MF and DMM is produced from each catalyst with no discernable dependence on VO_x loading or preparation method. In contrast to the low VO_x loading catalysts, the method of deposition has a significant effect on MeOH ODH of the near monolayer catalysts. The increased VO_x dispersion as a result of carefully controlled chemical grafting creates a more active catalyst despite the VO_x loading approaching near monolayer coverage with increased selectivity to CH_2O.

4 Conclusions

Deposition of VO_x on well-defined CeO_2 nanocubes supports was compared using conventional incipient wetness impregnation and liquid phase atomic layer deposition to explore the influence of preparation method on the structure of the supported VO_x and the resulting catalytic redox performance. At low VO_x loadings (i.e., 1 V/nm^2), well-dispersed monomers were detected on both samples which displayed the greatest activity for methanol oxidative dehydrogenation to formaldehyde. When the VO_x loading is increased to near monolayer coverage (i.e., 5 V/nm^2), the catalysts prepared using chemical grafting demonstrate much enhanced VO_x dispersion which not only fully covers the defect sites on bare CeO_2, mitigating side reactions,

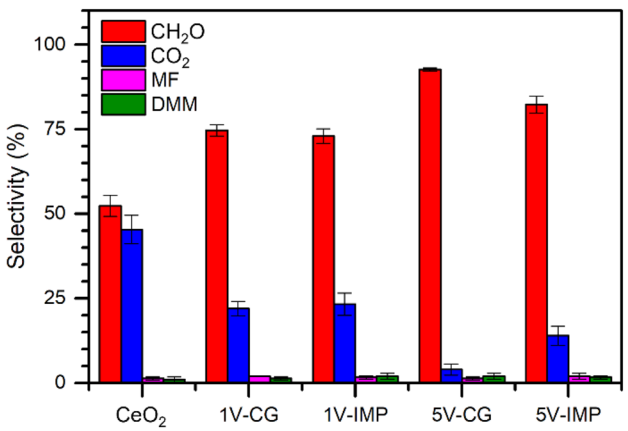

Fig. 9 Product selectivity during MeOH TPD at ~ 50% conversion for the CeO_2 nanocubes and VO_x/CeO_2 catalysts

but enhances the redox properties of these catalysts as well as increases activity of MeOH ODH in comparison to the samples prepared using impregnation. In addition, chemical grafting mitigates the formation of $CeVO_4$ for VO_x loadings above monolayer coverage due to a smaller fraction of VO_x oligomers. As we strive to develop fundamental structure–function relationships for supported metal oxide catalysts, precise control of both the support and deposited material is crucial. This study demonstrates that this liquid phase chemical grafting technique improves the dispersion of supported VO_x, allowing for more uniform reaction sites for future investigations.

Supplementary Information The online version contains supplementary material available at https://doi.org/10.1007/s10562-021-03862-8.

Funding This work was supported by U.S. Department of Energy (DOE), Office of Basic Energy Sciences, Division of Chemical Sciences, Geosciences, and Biosciences for funding this project (DE-AC05-RL01830).

References

1. Deo G, Wachs IE (1994) Reactivity of supported vanadium-oxide catalysts—the partial oxidation of methanol. J Catal 146(2):323–334
2. Wachs IE, Weckhuysen BM (1997) Structure and reactivity of surface vanadium oxide species on oxide supports. Appl Catal A 157(1):67–90
3. Watling TC et al (1996) Oxidative dehydrogenation of propane over niobia supported vanadium oxide catalysts. Catal Today 28(1):139–145
4. Burcham LJ, Wachs IE (1999) The origin of the support effect in supported metal oxide catalysts: in situ infrared and kinetic studies during methanol oxidation. Catal Today 49(4):467–484
5. Dobler J, Pritzsche M, Sauer J (2005) Oxidation of methanol to formaldehyde on supported vanadium oxide catalysts compared to gas phase molecules. J Am Chem Soc 127(31):10861–10868
6. Martinez-Huerta MV et al (2007) Changes in ceria-supported vanadium oxide catalysts during the oxidative dehydrogenation of ethane and temperature-programmed treatments. J Phys Chem C 111(50):18708–18714
7. Wachs IE (2011) The generality of surface vanadium oxide phases in mixed oxide catalysts. Appl Catal a Gen 391(1–2):36–42
8. Wachs IE (2013) Catalysis science of supported vanadium oxide catalysts. Dalton Trans 42(33):11762–11769
9. Zhu H et al (2015) VO_x/SiO_2 catalyst prepared by grafting $VOCl_3$ on silica for oxidative dehydrogenation of propane. ChemCatChem 20:3332–3339
10. Burcham LJ, Badlani M, Wachs IE (2001) The origin of the ligand effect in metal oxide catalysts: novel fixed-bed in situ infrared and kinetic studies during methanol oxidation. J Catal 203(1):104–121
11. Bond GC, Tahir SF (1991) Vanadium oxide monolayer catalysts preparation, characterization and catalytic activity. Appl Catal 71(1):1–31
12. Weckhuysen BM, Jehng JM, Wachs IE (2000) In situ Raman spectroscopy of supported transition metal oxide catalysts: O-18(2)-O-16(2) isotopic labeling studies. J Phys Chem B 104(31):7382–7387

13. Wu Z, Dai S, Overbury SH (2010) Multiwavelength Raman spectroscopic study of silica-supported vanadium oxide catalysts. J Phys Chem C 114(1):412–422
14. Wu Z, Li M, Overbury SH (2012) A Raman spectroscopic study of the speciation of vanadia supported on ceria nanocrystals with defined surface planes. ChemCatChem 4(10):1653–1661
15. Wu Z et al (2011) Structure of vanadium oxide supported on ceria by multiwavelength Raman spectroscopy. J Phys Chem C 115(51):25368–25378
16. Wu Z (2014) Multi-wavelength Raman spectroscopy study of supported vanadia catalysts: structure identification and quantification. Chin J Catal 35(10):1591–1608
17. Busca G (1989) On the mechanism of methanol oxidation over vanadia-based catalysts: a FT-IR study of the adsorption of methanol, formaldehyde and formic acid on vanad. J Mol Catal 50(2):241–249
18. Huang H et al (2015) Catalytic combustion of chlorobenzene over VO_x/CeO_2 catalysts. J Catal 326:54–68
19. Wu W et al (2017) Methanol oxidation to formate on ALD-prepared VO_x/θ-Al_2O_3 catalysts: a mechanistic study. J Phys Chem C 121(48):26794–26805
20. Zhao C, Wachs IE (2008) Selective oxidation of propylene over model supported V_2O_5 catalysts: influence of surface vanadia coverage and oxide support. J Catal 257(1):181–189
21. Beck B et al (2012) Partial oxidation of ethanol on vanadia catalysts on supporting oxides with different redox properties compared to propane. J Catal 296:120–131
22. Vining WC, Strunk J, Bell AT (2012) Investigation of the structure and activity of $VO_x/CeO_2/SiO_2$ catalysts for methanol oxidation to formaldehyde. J Catal 285(1):160–167
23. Carrero CA et al (2013) Anomalous reactivity of supported V_2O_5 nanoparticles for propane oxidative dehydrogenation: influence of the vanadium oxide precursor. Dalton Trans 42(35):12644–12653
24. Ober P, Rogg S, Hess C (2020) Direct evidence for active support participation in oxide catalysis: multiple operando spectroscopy of VO_x/Ceria. ACS Catal 5:2999–3008
25. Cousin R et al (1999) V-51 MAS NMR characterization of V-Ce-O catalysts. Colloids Surf a Physicochem Eng Aspects 158(1–2):43–49
26. Cousin R et al (2007) Physico-chemical study of impregnated Cu and V species on CeO_2 support by thermal analysis, XRD, EPR, V-51-MAS-NMR and XPS. J Mater Sci 42(15):6188–6196
27. Grant J et al (2015) Enhanced two-dimensional dispersion of group V metal oxides on silica. ACS Catal 10:5787–5793
28. Vining WC et al (2010) An experimental and theoretical investigation of the structure and reactivity of bilayered $VO_x/TiO_x/SiO_2$ catalysts for methanol oxidation. J Catal 270(1):163–171
29. Reddy BM, Lakshmanan P, Khan A (2004) Investigation of surface structures of dispersed V_2O_5 on CeO_2-SiO_2, CeO_2-TiO_2, and CeO_2-ZrO_2 mixed oxides by XRD, Raman, and XPS techniques. J Phys Chem B 108(43):16855–16863
30. Shapovalov V, Metiu H (2007) VO_x (x=1-4) submonolayers supported on rutile TiO_2(110) and CeO_2(111) surfaces: the structure, the charge of the atoms, the XPS spectrum, and the equilibrium composition in the presence of oxygen. J Phys Chem C 111(38):14179–14188
31. Liu J et al (2014) Origin of the high activity of mesoporous CeO_2 supported monomeric VO_x for low-temperature gas-phase selective oxidative dehydrogenation of benzyl alcohol: role as an electronic "hole." J Phys Chem C 118(43):24950–24958
32. Baron M et al (2009) Resolving the atomic structure of vanadia monolayer catalysts: monomers, trimers, and oligomers on ceria. Angew Chem-Int Ed 48(43):8006–8009
33. Vohs JM, Feng T, Wong GS (2003) Comparison of the reactivity of high-surface area, monolayer vanadia/ceria catalysts with vanadia/CeO(2)(111) model systems. Catal Today 85(2–4):303–309
34. Feng T, Vohs JM (2004) A TPD study of the partial oxidation of methanol to formaldehyde on CeO_2-supported vanadium oxide. J Catal 221(2):619–629
35. Baldychev I, Vohs JM, Gorte RJ (2011) The effect of support on redox properties and methanol-oxidation activity of vanadia catalysts. Appl Catal a Gen 391(1–2):86–91
36. Kim T, Wachs IE (2008) CH_3OH oxidation over well-defined supported V_2O_5/Al_2O_3 catalysts: Influence of vanadium oxide loading and surface vanadium–oxygen functionalities. J Catal 255(2):197–205
37. Wong GS, Concepcion MR, Vohs JM (2002) Oxidation of methanol to formaldehyde on vanadia films supported on CeO_2(111). J Phys Chem B 106(25):6451–6455
38. Abbott HL et al (2010) Relating methanol oxidation to the structure of ceria-supported vanadia monolayer catalysts. J Catal 272(1):82–91
39. Ganduglia-Pirovano MV et al (2010) Role of ceria in oxidative dehydrogenation on supported vanadia catalysts. J Am Chem Soc 132(7):2345–2349
40. Popa C, Ganduglia-Pirovano MV, Sauer J (2011) Periodic density functional theory study of VOn species supported on the CeO_2(111) surface. J Phys Chem C 115(15):7399–7410
41. Penschke C, Paier J, Sauer J (2018) Vanadium oxide oligomers and ordered monolayers supported on CeO_2(111): structure and stability studied by density functional theory. J Phys Chem C 122(16):9101–9110
42. Kropp T, Paier J, Sauer J (2017) Oxidative dehydrogenation of methanol at ceria-supported vanadia oligomers. J Catal 352:382–387
43. Yang S, Gao L (2006) Controlled synthesis and self-assembly of CeO_2 nanocubes. J Am Chem Soc 128(29):9330–9331
44. Yan L et al (2008) Template-free hydrothermal synthesis of CeO_2 nano-octahedrons and nanorods: Investigation of the morpholog evolution. Cryst Growth Des 8(5):1474–1477
45. Li Y et al (2014) Effects of CeO_2 support facets on VO_x/CeO_2 catalysts in oxidative dehydrogenation of methanol. J Catal 315:15–24
46. Wu Z et al (2012) Probing the surface sites of CeO2 nanocrystals with well-defined surface planes via methanol adsorption and desorption. ACS Catal 2(11):2224–2234
47. Machej T et al (1991) Monolayer V_2O_5/TiO_2 and MoO_3/TiO_2 catalysts prepared by different methods. Appl Catal 70(1):115–128
48. Haber J et al (1995) Mechanism of surface spreading in vanadia-titania system. Catal Lett 32(1):101–114
49. Keranen J et al (2001) Calorimetric measurements of the acidity of supported vanadium oxides prepared by ALE and impregnation. Thermochim Acta 379(1–2):233–239
50. Choi SM et al (2000) Cs-substituted tungstophosphoric acid salt supported on mesoporous silica. Catal Today 55(1–2):117–124
51. Wang Y, Peden CHF, Choi S (2001) Preparation of highly dispersed Cs-tungstophosphoric acid salt on MCM-41 silica. Catal Lett 75(3–4):169–173
52. Herrera JE et al (2006) Synthesis, characterization, and catalytic function of novel highly dispersed tungsten oxide catalysts on inesoporous silica. J Catal 239(1):200–211
53. Herrera JE et al (2006) Synthesis of nanodispersed oxides of vanadium, titanium, molybdenum, and tungsten on mesoporous silica using atomic layer deposition. Top Catal 39(3–4):245–255
54. Högerl MP et al (2018) SOMC grafting of vanadium oxytriisopropoxide (VO(OiPr)3) on dehydroxylated silica; analysis of surface complexes and thermal restructuring mechanism. RSC Adv 8(37):20801–20808

55. Barman S et al (2016) Single-site VO_x moieties generated on silica by surface organometallic chemistry: a way to enhance the catalytic activity in the oxidative dehydrogenation of propane. ACS Catal 6(9):5908–5921
56. Li Y et al (2015) Effect of oxygen defects on the catalytic performance of VO_x/CeO_2 catalysts for oxidative dehydrogenation of methanol. ACS Catal 5(5):3006–3012
57. Mai HX et al (2005) Shape-selective synthesis and oxygen storage behavior of ceria nanopolyhedra, nanorods, and nanocubes. J Phys Chem B 109(51):24380–24385
58. Mann AKP et al (2014) Adsorption and reaction of acetaldehyde on shape-controlled CeO_2 nanocrystals: elucidation of structure-function relationships. ACS Catal 4(8):2437–2448
59. Taniguchi T et al (2009) Identifying defects in ceria-based nanocrystals by UV resonance raman spectroscopy. J Phys Chem C 113(46):19789–19793
60. Wu Z et al (2012) Support shape effect in metal oxide catalysis: ceria-nanoshape-supported vanadia catalysts for oxidative dehydrogenation of isobutane. J Phys Chem Lett 3(11):1517–1522
61. Deo G, Wachs IE (1991) Predicting molecular structures of surface metal oxide species on oxide supports under ambient conditions. J Phys Chem 95(15):5889–5895
62. Panchal V et al (2011) Zircon to monazite phase transition in $CeVO_4$: X-ray diffraction and Raman-scattering measurements. Phys Rev B. https://doi.org/10.1103/PhysRevB.84.024111
63. Martinez-Huerta MV et al (2004) Nature of the vanadia-ceria interface in V_5^+/CeO_2 catalysts and its relevance for the solid-state reaction toward $CeVO_4$ and catalytic properties. J Catal 225(1):240–248
64. Badri A, Binet C, Lavalley J-C (1996) An FTIR study of surface ceria hydroxy groups during a redox process with H2. J Chem Soc, Faraday Trans 92(23):4669–4673
65. Binet C, Daturi M, Lavalley J-C (1999) IR study of polycrystalline ceria properties in oxidised and reduced states. Catal Today 50(2):207–225
66. Mullins DR, Robbins MD, Zhou J (2006) Adsorption and reaction of methanol on thin-film cerium oxide. Surf Sci 600(7):1547–1558
67. Siokou A, Nix RM (1999) Interaction of methanol with well-defined ceria surfaces: Reflection/absorption infrared spectroscopy, X-ray photoelectron spectroscopy, and temperature-programmed desorption study. J Phys Chem B 103(33):6984–6997
68. Gu X et al (2006) Structural, redox and acid–base properties of V_2O_5/CeO_2 catalysts. Thermochim Acta 451(1):84–93
69. Goodrow A, Bell AT (2008) A theoretical investigation of the selective oxidation of methanol to formaldehyde on isolated vanadate species supported on titania. J Phys Chem C 112(34):13204–13214